iScience, Volume *23*

Supplemental Information

Model to Link Cell Shape and Polarity with Organogenesis

Bjarke Frost Nielsen, Silas Boye Nissen, Kim Sneppen, Joachim Mathiesen, and Ala Trusina

Supplementary Figures

Figure S1 Budding outcomes in the absence of wedging. Related to Fig 2.

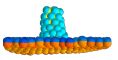

	Normal	Failed	Misoriented
High Noise σ = 0.1 N = 50	40%	0%	60%
Low Noise σ = 0.002 N = 50	20%	50%	30%
No Noise σ = 0 N = 50	0%	100%	0%

Budding outcomes without wedging at high and low noise as well as in the absence of noise. The first column shows the proportion of normal initiations of tubulation, the middle column shows failed invaginations while the last column shows evaginations. σ is the width of the Gaussian noise, while N is the number of simulations run at the given noise level. See the Methods section for details on the implementation of noise. In all cases $\mathrm{d}t = 0.1$. The couplings were kept at $(\lambda_1, \lambda_2, \lambda_3) = (0.4, 0.5, 0.1)$ and the annulus within which wedging occurs is given by the radii $r_0 = 5$ and $r_1 = 10$. Since wedging is absent, $\alpha = 0$.

Figure S2 Lack of proliferation. Related to Fig 4.

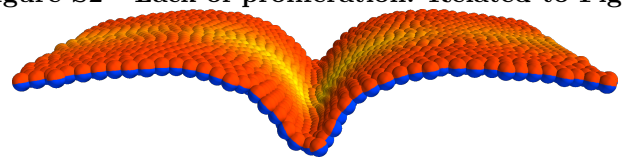

The fate of the neural sheet in our simulations in the absence of proliferation. Here the couplings are $(\lambda_1, \lambda_2, \lambda_3) = (0.6, 0.4, 0)$, the degree of wedging is $|\alpha| = 0.5$. See the section *Modeling neurulation/wrapping* for details. Total number of time steps was 1.4×10^5 at $\mathrm{d}t = 0.1$. The simulation was run without noise.

Figure S3 T1 transition induced by wedging. Related to Fig 1.

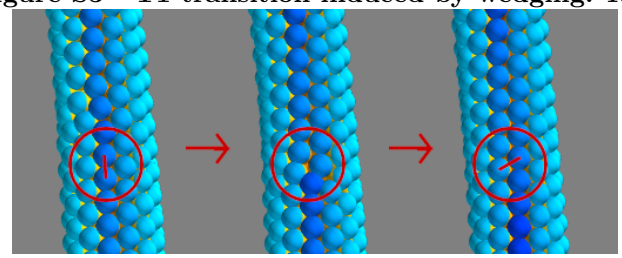

The T1 transition was induced by starting with a tube which was stabilized with anisotropic wedging of strength $|\alpha| = 0.3$ and then increasing the extent of wedging to $|\alpha| = 0.5$, causing the structure to tighten and elongate by intercalation. The couplings are $(\lambda_1, \lambda_2, \lambda_3) = (0.55, 0.45, 0)$ and the width of the Gaussian noise is 0.1 with time step size $\mathrm{d}t = 0.2$.

Figure S4 The initial configuration of the cell sheet for neurulation. Related to Fig 2.

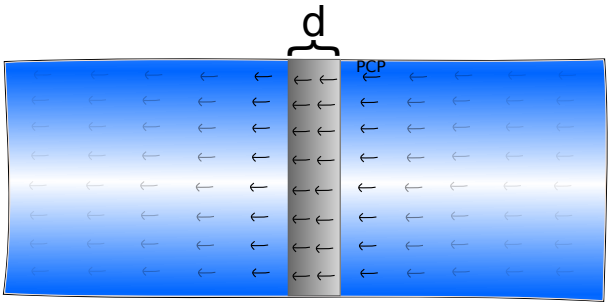

The initial configurations of the cell sheet for neurulation. Wedging is turned on in a band of width d (gray) with PCP running orthogonal to this band.

Figure S5 The initial configuration of the cell sheet for budding. Related to Fig 2.

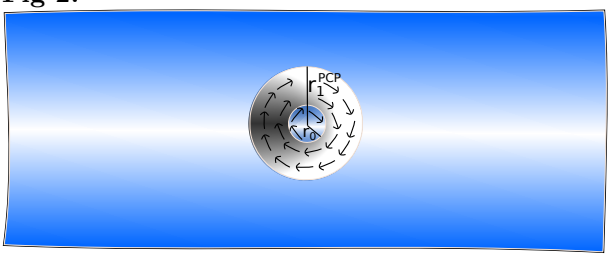

The initial configurations of the cell sheet for budding. Wedging is turned on in an annulus (gray) where PCP curls around tangentially.

Figure S6 Tube splitting observed with excessive proliferation rate. Related to Fig 4. The proliferation rate corresponds to a cell cycle length of 1.5h for cells at the neuroepithelium/ectoderm boundary. The remaining parameters are as in the main neurulation simulation, as described in Fig 2

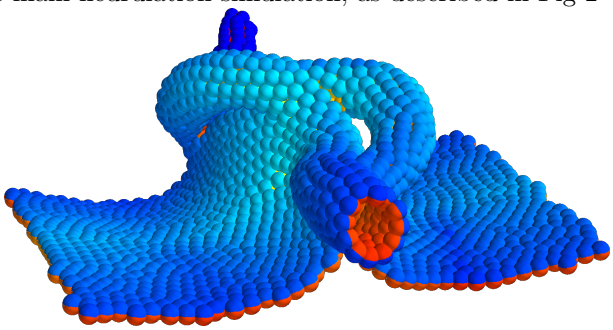

Figure S7 Influence of the parameter β. Related to Fig 2.

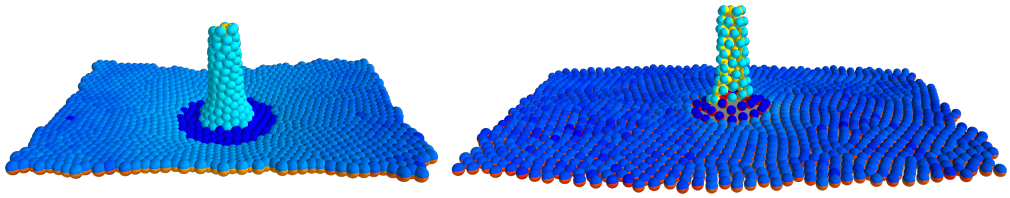

Budding simulations run with $\beta = 2.5$ (left) and $\beta = 10$ (right). This affects the equilibrium distance so that cells are closer together resp. further apart (and thus come across as larger resp. smaller) but budding progresses in a qualitatively similar manner.

The remaining simulations in this paper were all run with $\beta = 5$ ensuring an equilibrium distance of $d_{eq} = 2$.

Figure S8 Apical constriction in budding. Related to Fig 2.

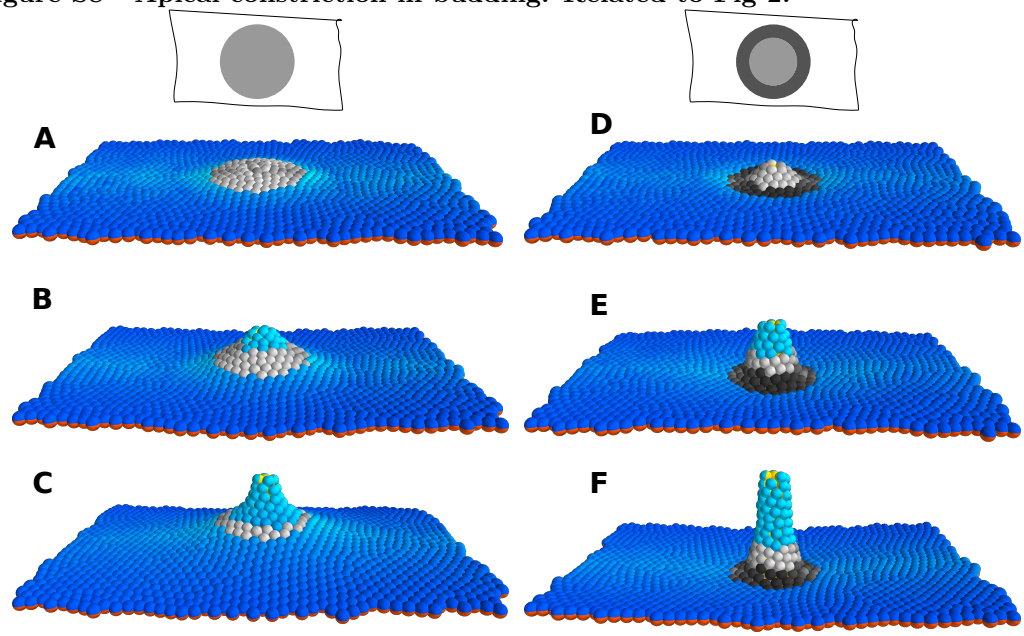

(**A-C**) Time evolution of budding simulation when only a disk of apically constricting cells (light gray) are assigned, and no basally contracting cells. The couplings are $(\lambda_1, \lambda_2, \lambda_3) = (0.5, 0.4, 0.1)$, the degree of wedging is $|\alpha| = 0.3$. The radius of the disk of apically constricting cells is given by $r_0 = 10$. Total number of time steps was 6.8×10^4 at $\mathrm{d}t = 0.1$. Snapshots correspond to times 175, 600 and 6800.

(**D-F**) Time evolution of budding simulation when a disk of apically constricting cells (light gray) as well as a ring of basally constricting cells (dark gray) are assigned. The couplings are $(\lambda_1, \lambda_2, \lambda_3) = (0.5, 0.4, 0.1)$, the degree of wedging is $|\alpha| = 0.3$. The outer radius of the ring for which basal constriction occurs is given $r_1 = 10$ while the radius of the disk of apically constricting cells is given by $r_0 = 5$. Total number of time steps was 2.2×10^4 at $\mathrm{d}t = 0.1$. Snapshots correspond to times 25, 400 and 2200.

Figure S9 The degree of wedging affects the circumference of the tube. Related to Fig 1.

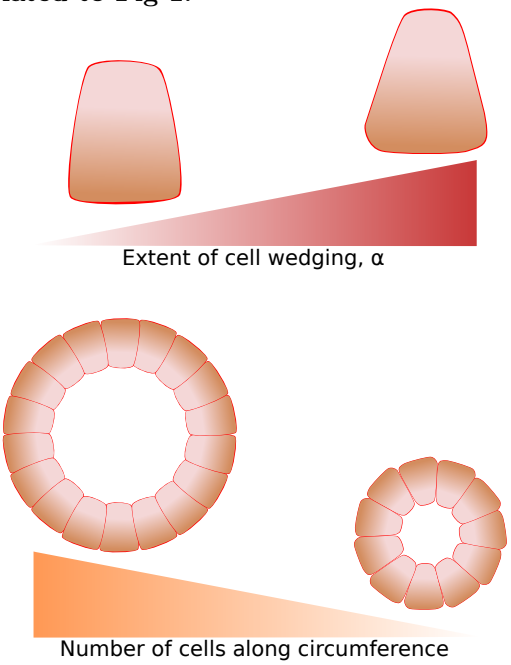

Transparent Methods

Model

Following Nissen et al. (2018), cells are treated as point particles interacting with neighboring cells through a pair-potential V_{ij}. The potential has a rotationally symmetric repulsive term and a polarity-dependent attractive term. In terms of r_{ij} (the distance between two cells i and j), the dimensionless potential can be formulated as

$$V_{ij} = e^{r_{ij}} - [\lambda_1 \, S_{ij}(A) + \lambda_2 \, S_{ij}(AP) + \lambda_3 \, S_{ij}(P)] \, e^{-r_{ij}/\beta}. \tag{S1}$$

The parameter β has the fixed value $\beta = 5$, since this ensures that the equilibrium distance is always 2, corresponding to 2 cell radii. In Figure S7 we have shown that one can obtain qualitatively similar results at other values of β. The parameters λ_i are coupling constants which define the strength of polar interactions in the model. $S_{ij}(A)$ gives the form of the interaction between AB polarity and position, whereas $S_{ij}(AP)$ and $S_{ij}(P)$ give the coupling of PCP with AB and position, respectively, as described in Nissen et al. (2018). These couplings are formulated in terms of AB vectors $\mathbf{p}_i$, PCP vectors $\mathbf{q}_i$ and a unit vector $\hat{\mathbf{r}}_{ij}$ from cell i to j. The coupling $S_{ij}(AP) = (\mathbf{p}_i \times \mathbf{q}_i) \cdot (\mathbf{p}_j \times \mathbf{q}_j)$ dynamically maintains the orthogonality of the PCP unit vectors $\mathbf{q}_i$ and $\mathbf{q}_j$ to their corresponding AB polarity vectors while lateral organization is favored by $S_{ij}(P) = (\hat{\mathbf{r}}_{ij} \times \mathbf{q}_i) \cdot (\hat{\mathbf{r}}_{ij} \times \mathbf{q}_j)$. In the absence of any cell shape effects, the coupling between AB and position is given by $S_{ij}(A) = (\hat{\mathbf{r}}_{ij} \times \mathbf{p}_i) \cdot (\hat{\mathbf{r}}_{ij} \times \mathbf{p}_j)$, which favors a flat cell sheet. Wedging of cells is introduced into our model by a single deformation parameter α, which describes an attractive interaction between the AB polarity unit vectors $\mathbf{p}_i$ and $\mathbf{p}_j$:

$$S_{ij}(A) = (\hat{\mathbf{r}}_{ij} \times \tilde{\mathbf{p}}_i) \cdot (\hat{\mathbf{r}}_{ij} \times \tilde{\mathbf{p}}_j), \tag{S2}$$

where $\tilde{\mathbf{p}}_i$ is given by

$$\begin{aligned}
\tilde{\mathbf{p}}_i &= \mathbf{p}_i \quad \text{(for no wedging)}, \\
\tilde{\mathbf{p}}_i &= \frac{\mathbf{p}_i - \alpha \hat{\mathbf{r}}_{ij}}{|\mathbf{p}_i - \alpha \hat{\mathbf{r}}_{ij}|} \quad \text{(for isotropic wedging)}, \\
\tilde{\mathbf{p}}_i &= \frac{\mathbf{p}_i - \alpha \langle \hat{\mathbf{q}} \rangle_{ij}}{|\mathbf{p}_i - \alpha \langle \hat{\mathbf{q}} \rangle_{ij}|} \quad \text{(for anisotropic wedging)}.
\end{aligned} \tag{S3}$$

Here, $\langle \hat{\mathbf{q}} \rangle_{ij}$ denotes the mean of PCP vectors $\mathbf{q}_i$ and $\mathbf{q}_j$ belonging to the two interacting cells. The above substitution, $\mathbf{p}_i \to \tilde{\mathbf{p}}_i$, is only performed in $S_{ij}(A)$, so as to only affect the coupling between AB polarity and position.

Setting $\alpha = 0$ favors a flat sheet (see Fig 1A–B) whereas a non-zero α favors bending of AB polarity vectors towards (or away from) one another and induces curvature in a sheet of cells (Fig 1C–D).

The time development is simulated by overdamped (relaxational) dynamics along the gradient of the above potential, Eq (S1):

$$\begin{aligned}
\frac{\partial \mathbf{r}_i}{\partial t} &= -\frac{\partial V_i}{\partial \mathbf{r}_i} + \eta, \\
\frac{\partial \mathbf{p}_i}{\partial t} &= -\frac{\partial V_i}{\partial \mathbf{p}_i} + \eta, \\
\frac{\partial \mathbf{q}_i}{\partial t} &= -\frac{\partial V_i}{\partial \mathbf{q}_i} + \eta,
\end{aligned} \tag{S4}$$

where the potential energy function for the i'th cell is $V_i = \sum_j V_{ij}$. The sum runs over those cells j which are within direct line of sight of the i'th cell as described in Nissen et al. (2018). η is a noise term corresponding to Gaussian white noise with vanishing mean. This noise term provides a degree of randomness to cell position as well as the orientation of polarities. Cell division (when present) is modeled as a Poisson process with daughter cells being placed randomly around the mother cell at a distance of one cell radius.

The model was implemented in Python using PyTorch for automatic differentiation (Paszke et al. 2017). Numerical integration of the equations of motion is implemented through the Euler method, usually with $\mathrm{d}t = 0.1$. We have checked that the model converges to similar results (tested for budding) with $\mathrm{d}t = 10^{-4}$. The source code for the simulations is available on GitHub (Nielsen 2019).

Parameter estimation and robustness

We have tested the robustness of our approach on a number of model cases and find that, for example, *budding* can be reproduced with a broad range of wedging parameters, $\alpha \in [0.1, 0.6]$ and for diverse PCP coupling strengths $\lambda_3 \in [0.8, 0.14]$. For these intervals, the budding is qualitatively similar to that illustrated in Fig 2A. Our typical values of wedging used in simulations, $\alpha \in [0.3, 0.5]$ are comparable with the wedging strains reported in Sanchez-Corrales et al. (2018), e.g. $0.03pp/\mu\mathrm{m}$, corresponding to $\alpha = 0.4$ (assuming a cell diameter of 13µm) (Brown & Bron 1987).

We further explore our model by re-instating dimensions in the formulation of the potential and the equation of motion and estimating dimensionful quantities. With dimensions reinstated, the pair-potential takes the form

$$V_{ij} = V_0 \left[\exp(-r/\ell) - S \exp(-r/(\beta\ell)) \right]. \tag{S5}$$

The overdamped equation of motion (without noise) becomes

$$0 = \gamma \mathbf{v}_i + \frac{\partial V_{ij}}{\partial \mathbf{r}_i}, \tag{S6}$$

where $\mathbf{v}_i = \partial \mathbf{r}_i / \partial t$. We now introduce dimensionless (tilded) parameters

$$V_{ij} = V_0 \tilde{V}_{ij}, \quad \mathbf{r}_i = \ell \tilde{\mathbf{r}}_i, \quad v_i = v_0 \tilde{v}_i = \frac{\ell}{t_0} \tilde{v}_i. \tag{S7}$$

and insert the dimensionless parameters in our equation of motion

$$\tilde{\mathbf{v}}_i = -\frac{V_0}{\ell \gamma v_0} \frac{\partial \tilde{V}_{ij}}{\partial \tilde{\mathbf{r}}_i}. \tag{S8}$$

Inserting the dimensionless equation of motion, this reduces to $V_0 = \ell \gamma v_0$. In Eskandari & Salcudean (2008), a typical value for the dynamical viscosity μ was reported to be on the order of 250Pa s. This can be related to the coefficient γ by Stokes' Law of viscous drag, $\gamma = 6\pi\mu\ell$. We now compare our model with epithelial cell extrusion and use the typical cell speed reported in Yamada et al. (2017), $v_0 \approx 1\text{mm}\,\text{h}^{-1}$ and use the typical cell size reported in Brown & Bron (1987), $2\ell = 13\mu\text{m}$. With these numbers, our model predicts a typical extrusion energy on the order of

$$12V_0 \approx 12 \times 6\pi\mu\ell^2 v_0 \approx 2 \times 10^{-13}\text{J}. \tag{S9}$$

The factor of $12 = 2 \times 6$ is due to the hexagonal structure of the cell sheet. Note that our estimate of the extrusion energy is consistent with the finding in Yamada et al. (2017) for epithelial cell extrusion. Here, an actomyosin ring is measured to exhibit a contraction force of the order of 1kPa, which results in an extrusion energy of the order $1\text{kPa} \times \ell^3 \approx 3 \times 10^{-13}\text{J}$.

With these identifications of parameters, it is possible to extract dimensionful quantities from our simulations. This is what allows for e.g. the computation of cell cycle lengths in Fig 4.

We anticipate that the values of the couplings λ_i can be estimated from the extent and speed of CE (e.g in our model these would be determined by the values of λ_3 relative to λ_1).

Modeling neurulation/wrapping

The starting point for our simulation of neurulation is a planar sheet of cells where a line with a width of six cell radii is given non-zero wedging strength $|\alpha| = \alpha_0 > 0$ and all other cells have $\alpha = 0$. The line is centered at $x = 0$ and PCP is initialized orthogonally to this line, along the x direction ($\mathbf{q}|_{t=0} = \hat{\mathbf{x}}$). See Figure S4.

Cell proliferation is simulated as a Poisson process by choosing a rate Γ for *each cell* to divide in each time unit. Only cells at the neuroepithelium-ectoderm boundary (defined as cells with $|\alpha| > 0$ who are neighbours of cells with $\alpha = 0$) proliferate (with rate $\Gamma = \Gamma_0 > 0$) while the rest have $\Gamma = 0$. Daughter cells inherit all properties of their mother cell and are initiated randomly in a distance of one cell radius from their mother cell.

It should be noted that the initial width of the strip is not particularly important, since wedging will ensure the correct tube width given sufficient proliferation.

All cells in the simulation have the same coupling constants, typically $\lambda = (0.6, 0.4, 0)$. Typical values for Γ_0 and α_0 are 2.8×10^{-4} and 0.5. respectively.

Modeling gastrulation

In our gastrulation simulation, the assignment of PCP and cell wedging is characterized by two radii, describing an annulus (see Figure S5):

$$r_0 = 7, \tag{S10}$$

$$r_1 = 3r_0 = 21. \tag{S11}$$

PCP is assigned within the disk Ω_1 given by

$$\Omega_1 = \left\{ (x, y, z) \,\middle|\, \sqrt{x^2 + y^2} < r_1 \right\}. \tag{S12}$$

The PCP coupling strength λ is taken to be

$$\lambda = \begin{cases} (0.5, 0.5 - \lambda_3, \lambda_3) & \text{inside } \Omega_1, \\ (1, 0, 0) & \text{everywhere else.} \end{cases} \tag{S13}$$

where a typical value for λ_3 is between 0.08 and 0.12.

The PCP vector field $\mathbf{q}$ is initially assigned so that it spirals around the axis of tube formation (the z-axis):

$$\mathbf{q}|_{t=0} = \hat{\boldsymbol{z}} \times \mathbf{r}, \tag{S14}$$

In the gastrulation simulations, the PCP vector field is fixed on a per-cell basis.

Nonzero apical constriction parameter α is assigned in an annulus Ω_2, which shares its outer radius with the disk Ω_1:

$$\Omega_2 = \left\{ (x, y, z) \,\middle|\, r_0 < \sqrt{x^2 + y^2} < r_1 \right\}. \tag{S15}$$

The magnitude of α for the cells in Ω_2 is taken as 0.4:

$$|\alpha| = \begin{cases} 0.4 & \text{inside } \Omega_2, \\ 0 & \text{everywhere else.} \end{cases} \tag{S16}$$

The regions Ω_1 and Ω_2 are fixed in space and not on a particle basis. The number of particles in this simulation is $N = 4000$.

Modeling budding from plane

The budding simulation is, apart from global topology, very similar to the gastrulation simulation.

The relevant length parameters are r_0 and r_1 with $r_0 < r_1$. Typically we take

$$r_0 = 5, \tag{S17}$$

$$r_1 = 2r_0 \text{ or } r_1 = 3r_0. \tag{S18}$$

Two regions are correspondingly defined – the disk Ω_1 and the annulus Ω_2:

$$\Omega_1 := \left\{ (x, y, z) \,\middle|\, \sqrt{x^2 + y^2} < r_1 \right\}, \tag{S19}$$

$$\Omega_2 := \left\{ (x, y, z) \,\middle|\, r_0 < \sqrt{x^2 + y^2} < r_1 \right\}. \tag{S20}$$

The PCP coupling strength λ is taken to be

$$\lambda = \begin{cases} (0.5, 0.5 - \lambda_3, \lambda_3) & \text{inside } \Omega_1, \\ (1, 0, 0) & \text{everywhere else.} \end{cases} \tag{S21}$$

where a typical value for λ_3 is between 0.08 and 0.12.

The PCP vector field $\mathbf{q}$ is initially assigned so that it spirals around the center of invagination (the origin of coordinates):

$$\mathbf{q}|_{t=0} = \hat{\boldsymbol{z}} \times \mathbf{r}, \tag{S22}$$

In the gastrulation simulations, the PCP vector field is fixed on a per-cell basis.

Nonzero apical constriction parameter α is assigned in the annulus Ω_2 with magnitude 0.5:

$$|\alpha| = \begin{cases} 0.5 & \text{inside } \Omega_2, \\ 0 & \text{everywhere else.} \end{cases} \tag{S23}$$

The total number of particles in the simulation is 1384.

References

Brown, N. & Bron, A. J. (1987), 'An estimate of the human lens epithelial cell size in vivo', *Experimental Eye Research* **44**(6), 899–906.

Eskandari, H. & Salcudean, S. E. (2008), Characterization of the viscosity and elasticity in soft tissue using dynamic finite elements, *in* '2008 30th Annual International Conference of the IEEE Engineering in Medicine and Biology Society', IEEE, pp. 5573–5576.

Nielsen, B. F. (2019), 'OrganogenesisPCP', `https://github.com/BjarkeFN/OrganogenesisPCP`.

Nissen, S. B., Rønhild, S., Trusina, A. & Sneppen, K. (2018), 'Theoretical tool bridging cell polarities with development of robust morphologies', *eLife* **7**, e38407.

Paszke, A., Gross, S., Chintala, S., Chanan, G., Yang, E., DeVito, Z., Lin, Z., Desmaison, A., Antiga, L. & Lerer, A. (2017), 'Automatic differentiation in pytorch'.

Sanchez-Corrales, Y. E., Blanchard, G. B. & Röper, K. (2018), 'Radially patterned cell behaviours during tube budding from an epithelium', *eLife* **7**, e35717.

Yamada, S., Iino, T., Bessho, Y., Hosokawa, Y. & Matsui, T. (2017), 'Quantitative analysis of mechanical force required for cell extrusion in zebrafish embryonic epithelia', *Biology Open* **6**(10), 1575–1580.